Revue des Composites et des Matériaux Avancés-Journal of Composite and Advanced Materials
Vol. 36, No. 5, October, 2026, pp. 1053-1059
Journal homepage: http://iieta.org/journals/rcma

Constructing High Efficiency ZnO Nanorods/BODIPY Hybrid Compounds for Field-Induced Fluorescence Enhancement

Ahmed Namah Mohamed[1*], Jafer Fahdel Odah[2]

[1] Department of Physics, College of Science, Al-Muthanna University, Samawah 66001, Iraq
[2] Department of Medical Physics, College of Science, Al-Karkh University of Science, Baghdad 10001, Iraq

Corresponding Author Email: ahmednamah@mu.edu.iq

Copyright: ©2026 The authors. This article is published by IIETA and is licensed under the CC BY 4.0 license (http://creativecommons.org/licenses/by/4.0/).

https://doi.org/10.18280/rcma.360512

Received: 6 July 2026
Revised: 27 August 2026
Accepted: 16 September 2026
Available online: 31 October 2026

Keywords:
ZnO nanorods, boron dipyrromethene dye, fluorescence, localized electromagnetic field, hybrid nanostructures, optical spectroscopy

ABSTRACT

Synthetic ZnO nanorods/boron dipyrromethene (BODIPY) hybrid compounds were prepared to investigate field-induced fluorescence enhancement. Hexagonal wurtzite ZnO nanorods, synthesized via a hydrothermal method, were combined with BODIPY dye solutions across a ZnO loading range of 0.5 to 2.5 mg. Structural and morphological characterizations confirmed the c-axis preferential growth of uniform ZnO nanorods. Spectroscopic evaluations revealed that BODIPY maintained discrete absorption spectra with small Stokes shifts across the tested concentration range. Incorporating ZnO nanorods significantly increased both absorption and fluorescence intensities. The fluorescence enhancement factor scaled with ZnO loading, reaching a maximum enhancement factor of 1.54 (a 53.78% increase in fluorescence intensity) at a loading of 2.5 mg ZnO. This optical enhancement is primarily attributed to localized electromagnetic field effects produced by the ZnO nanorods, alongside potential contributions from light scattering and interfacial interactions. Within the investigated loading range, a strong linear correlation (R2 = 0.98) was established between ZnO concentration and fluorescence intensity, demonstrating the operational tunability of the hybrid system.

1. INTRODUCTION

Semiconductor nanostructures have appealed to scientific interest over the past decades because of their exceptional optical properties which differ from those of bulk materials [1]. Among these nanomaterials, ZnO has emerged as one of the most promising semiconductor materials because of its wide direct band gap (~3.37 eV), high exciton binding energy (~60 meV), excellent chemical stability, low toxicity, and cost-effective synthesis routes [2]. One-dimensional ZnO nanostructures afford a high surface-to-volume ratio and can enhance the interaction between light and material, which makes them suitable for optoelectronic [3], sensing [4], photocatalytic [5], and fluorescence applications [6].

Boron dipyrromethene (BODIPY) dyes are an important type of organic fluorophores categorized by strong absorption coefficients, narrow emission bands, high fluorescence quantum yields and higher photostability [7, 8]. These properties make BODIPY products extremely attractive for applications in bio-imaging [9], optical sensing [10], fluorescence category [11], and photonic devices [12]. However, the fluorescence efficiency of BODIPY dye systems could be considerably affected by self-quenching, depending on concentration quenching and molecular aggregation effects, particularly at higher BODIPY dye concentrations [13, 14].

Hybrid organic/inorganic nanostructures have attracted significant attention as an effective approach for refining fluorescence performance through interfacial interaction and localized electromagnetic field improvement [15]. Combining semiconductor nanostructures with fluorescent organic BODIPY dyes can adapt the optical environment surrounding the fluorophore, that most important to enhance excitation (absorption) efficiency, improved radiative decay processing and conquest of non-radiative transitions [16]. In this context ZnO nanorods are predominantly attractive because their anisotropic morphology can successfully concentrate electromagnetic fields near the nanorod surface, thus increasing the interaction between incident photons and neighboring fluorescent molecules.

The current work aims to synthesize ZnO nanorods via a simple hydrothermal method and to explore the role of these nanostructures in enhancing the fluorescence phenomena of BODIPY dye through the creation of ZnO/BODIPY hybrid systems. The optical performance of the prepared hybrids was evaluated using ultraviolet–visible (UV–Vis) absorption and fluorescence spectroscopy. Specific highlighting was engaged to understand the mechanism of localized electromagnetic field-induced fluorescence enhancement through the analysis of enhancement factors, excitation efficiency, radiative decay behavior, and spectral broadening characteristics. The finding results give valued comprehensions into the development of

high efficient hybrid nanophotonic systems for innovative sensing and optoelectronics applications.

2. EXPERIMENTAL SECTION

Zinc oxide nanorods were synthesized via a hydrothermal method using a home-made 100 mL Teflon-lined stainless-steel autoclave. All chemicals were of analytical grade and used as received from commercial suppliers (Sigma-Aldrich, 99% purity). The starting raw material was commercial ZnO powder with an average particle size of ~1–5 µm. The Teflon liner was immersed in a 20% hydrochloric acid solution for 10 min to remove contaminants, followed by thorough rinsing with deionized water. Glass substrates were cleaned in an ultrasonic bath using an ethanol: acetone mixture (1:1) and subsequently dried under ambient air conditions. In a typical synthesis, 2.0 g of the precursor ZnO powder was introduced into an aqueous solution of 3 M NaOH. The mixture was magnetically stirred at 27 ℃ for 1 h to form a homogeneous precursor suspension. The resulting mixture was transferred into the Teflon-lined autoclave, filled to 60 mL of its total capacity. The autoclave was sealed and maintained at a constant temperature of 70 ℃ for 24 h. After cooling naturally to room temperature, the synthesized ZnO nanorods were collected, washed repeatedly with deionized water and ethanol to remove residual ions, dried at 80 ℃ for 6 h, and ground into a fine powder. The reaction yielded approximately 1.85 g, corresponding to a yield of ~92.5% of ZnO nanorods.

To diminish molecular self-aggregation, a series of dilute BODIPY dye solutions (4,4-difluoro-1,3,5,7-tetramethyl-4-bora-3a,4a-diaza-s-indacene), obtained from Sigma-Aldrich (98% purity), was prepared in tetrahydrofuran (THF) within a concentration range of 10^{-6} to 10^{-2} mol/L. These solutions were characterized using UV–Vis spectroscopy and fluorescence spectroscopy to identify the optimal dye concentration displaying maximum emission intensity without self-quenching. A stable colloidal stock suspension of ZnO nanorods (1 mg/mL) was prepared by dispersing 10 mg of the synthesized ZnO powder in 10 mL of THF under ultrasonic agitation for 15–30 min. Hybrid dye–nanoparticle systems were subsequently fabricated by doping the optimized BODIPY solution with specific volumetric aliquots of the ZnO stock suspension to yield individual nanoparticle mass loadings of 0.5, 1.0, 1.5, 2.0, and 2.5 mg in the final mixture.

The crystalline phase of the hydrothermally synthesized ZnO nanorods was examined by X-ray diffraction (XRD), while their surface morphology and elemental composition were investigated using field emission scanning electron microscopy (FE-SEM) equipped with energy-dispersive X-ray spectroscopy (EDX). The electronic transitions of both the bare dye and the hybrid ZnO/BODIPY systems were recorded using a UV–Vis spectrophotometer in the wavelength range of 100–1100 nm. Fluorescence emission spectra were collected using a spectrofluorometer at the optimal excitation wavelength determined for the dye.

3. DISCUSSION OF RESULTS

The crystallinity of the hydrothermally synthesized ZnO nanorods was investigated using XRD, as shown in Figure 1. The diffraction pattern confirms the successful formation of crystalline ZnO with a hexagonal wurtzite structure.

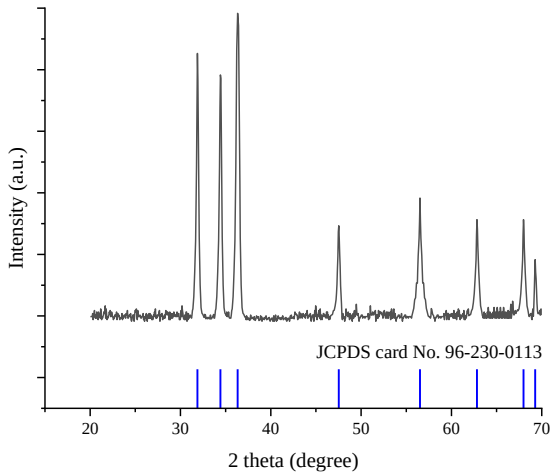


Figure 1. X-ray diffraction (XRD) pattern of hydrothermally synthesized ZnO nanorods

The diffraction peaks located at approximately 2θ = 31.7°, 34.4°, and 36.2° correspond to the (100), (002), and (101) crystallographic planes, respectively. The presence of these characteristic peaks matching standard JCPDS data confirms the phase purity of ZnO without noticeable secondary phases such as $Zn(OH)_2$ or impurities.

The main intensity (002) peak indicates growth orientation along the c-axis, which is a typical feature of one-dimensional ZnO nanorods. This preferential orientation is attributed to anisotropic growth along the [0001] direction, where surface energy minimization governs crystal elongation. The sharp and narrow diffraction peaks further confirm the high crystallinity and low defect density of the synthesized ZnO, which is the main cause for enhancing the optical performance in hybrid systems. This result agrees with literature reports where hydrothermally grown ZnO nanorods typically exhibit highly crystalline structures and no impurity phases, confirming the effectiveness of low-temperature hydrothermal synthesis in producing pure ZnO nanorods [17].

To rigorously quantify the crystallographic structural variations and meet peer-review expectations, the average volume-weighted crystallite size (D) was evaluated using Scherrer's formulation [18]:

$$D = \frac{K\lambda}{\beta \cos\theta} \quad (1)$$

where, K = 0.9 represents the shape factor, λ = 0.15406 nm denotes the Cu-Kα X-ray wavelength, β is the full width at half maximum (FWHM) of the diffraction peak expressed in radians, and θ is the Bragg diffraction angle. The calculated structural metrics are compiled in Table 1.

The structural parameters, including peak positions (2θ), interplanar spacing (d), FWHM, and calculated crystallite sizes (D) for the main diffraction planes, are quantitatively summarized in Table 1.

The XRD structural parameters calculated for the synthesized ZnO nanorods are quantitatively summarized in Table 1. The average crystallite size (D) calculated across the reflection planes using Scherrer's equation is approximately 26.70 nm, with the largest crystallite size (32.3 nm) observed along the (002) plane. The calculated lattice parameters (a = b = 3.250 Å and c = 5.206 Å) show excellent agreement with the standard hexagonal wurtzite ZnO data (JCPDS card No. 96-230-0113). Furthermore, the high relative intensity ratio of

I(002)/I(100) = 1.28 quantitatively confirms the preferential crystal growth along the c-axis, which facilitates effective field-induced optical interactions in the hybrid system.

Table 1. Quantitative X-ray diffraction (XRD) structural parameters, crystallite sizes, and lattice constants of hydrothermally synthesized ZnO nanorods

Plane (hkl)	2θ Observed (Degree)	d-Spacing Å	FWHM β (Degree)	Crystallite Size (D nm)
100	31.75	2.816	0.28	29.8
002	34.42	2.603	0.26	32.3
101	36.25	2.476	0.31	27.2
102	47.54	1.911	0.33	26.5
110	56.6	1.625	0.35	25.8
103	62.86	1.476	0.38	24.5
112	67.96	1.378	0.4	23.9
201	69.1	1.358	0.41	23.5

Note: Full width at half maximum (FWHM).

The surface morphology of ZnO nanorods was examined using FE-SEM as shown in Figure 2. The micrographs show the formation of distinct and rod-like nanostructures with comparatively uniform size distribution and high surface density.

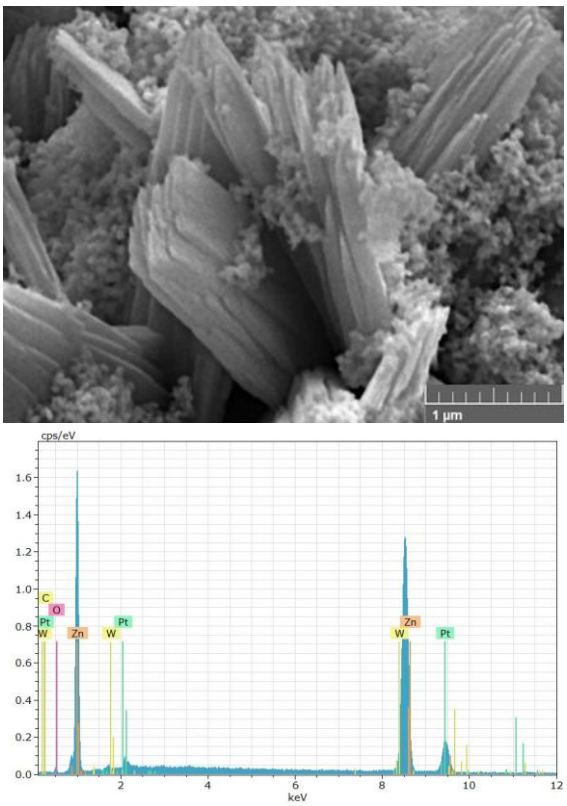


Figure 2. Field emission scanning electron microscopy (FE-SEM) images and energy-dispersive X-ray spectroscopy (EDX) spectrum of ZnO nanorods

The nanorods in FE-SEM image display elongated one dimension morphology ranged at arbitrary orientations an average length of 1.5 ± 0.3 µm and a mean diameter of 115 ± 15 nm which improves surface area and supports strong interaction of light–matter. The smooth surface morphology and low agglomeration indicate control of the nucleation and growth during the hydrothermal process. This structure is highly useful for optical applications as it assists localized electromagnetic field enhancement around the nanorod surfaces.

The elemental composition was confirmed by EDX presented in the inset of Figure 2. The spectrum reveals only Zn and O peaks, confirming the high chemical purity of the nano-oxide. The absence of impurity peaks shows the efficient formation of ZnO without contamination. The stoichiometric Zn/O ratio indicates full oxidation during synthesis, while minor deviations can be attributed to oxygen vacancies commonly observed in ZnO nanorods. These defects may play a role in adapting electronic transitions through localized energy states within the band gap. This agrees with a report demonstrating that ZnO nanorods can amplify local electromagnetic fields and increase fluorescence in coupled organic fluorophores [19].

The absorption and fluorescence spectra of BODIPY dye at different concentrations (10^{-2}–10^{-6} mol/L) are presented in Figure 3, while the corresponding quantitative optical parameters are summarized in Table 2.

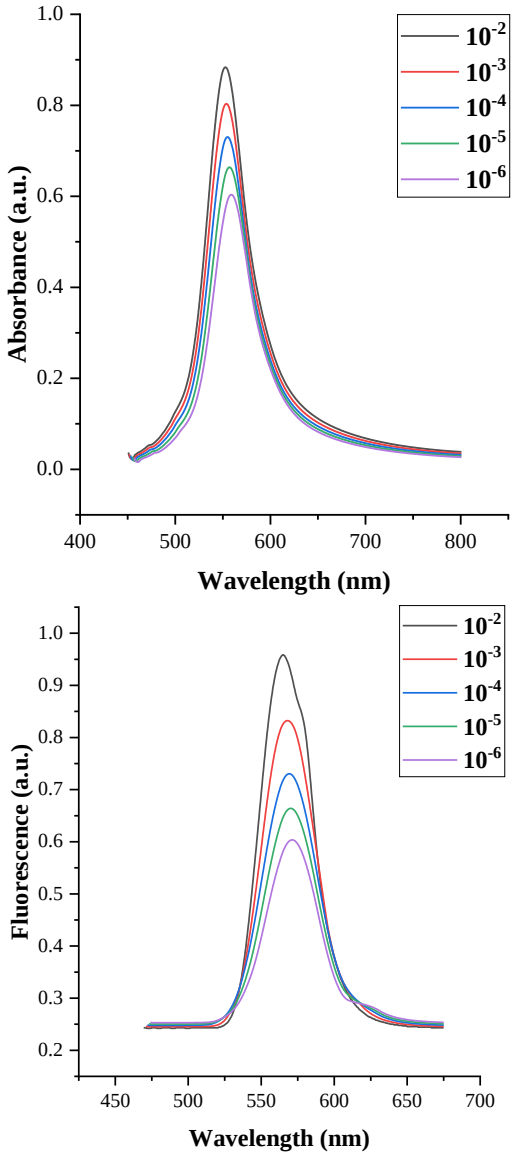


Figure 3. Ultraviolet–visible (UV–Vis) absorption and fluorescence spectra of boron dipyrromethene (BODIPY) dye at different concentrations (10^{-2}–10^{-6} mol/L)

The spectral shapes shown in Figure 3 show that absorption and fluorescence intensities are directly dependent on dye concentration. A decrease in peak intensity is observed as the concentration is reduced from 10^{-2} to 10^{-6} mol/L, indicating a direct relation between the number of absorbing/emitting molecules and the optical response of the dye. This conduct reflects the fundamental principles of light and matter interaction designated by the Beer–Lambert law, where the probability of photon absorption decreases proportionally with molecular concentration. Similar behavior has been reported in the literature for BODIPY products and related organic dyes, where absorption and fluorescence intensities scale linearly with concentration without significant deviation or nonlinear effects [20].

The quantitative optical parameters of BODIPY dye at various concentrations ranging from 10^{-2} to 10^{-6} mol/L are summarized in Table 2. This includes detailed characteristics such as the maximum intensity of absorption and fluorescence spectra, FWHM for absorption and fluorescence spectra, and the calculated Stokes shift values.

Table 2. Absorption and fluorescence characteristics of boron dipyrromethene (BODIPY) dye at different concentrations (10^{-2}–10^{-6} mol/L)

Concentration mol/L	Max. abs.	FWHM abs. nm)	Max. Flu.	FWHM Flu. (nm)	Stokes Shift (nm)
10^{-2}	0.88	56	0.96	38	11
10^{-3}	0.80	55	0.83	40	15
10^{-4}	0.73	54	0.73	43	14
10^{-5}	0.66	53	0.66	41	13
10^{-6}	0.60	52	0.60	40	12

Note: Full width at half maximum (FWHM).

The data listed in Table 2 confirm this tendency, where the absorption maximum decreases from 0.88 to 0.60 while the fluorescence maximum decreases from 0.96 to 0.60 with concentration. This reduction in absorption and fluorescence intensities indicates that the optical response of BODIPY scales linearly with concentration without any quenching or nonlinear effects. Also, the spectral shapes observed in Figure 3 remain unchanged for all concentrations, suggesting that the electronic transition of the BODIPY dye is preserved. This stability is supported by the constant (FWHM) values listed in Table 2, where the absorption bandwidth varies from 56 to 52 nm, and the fluorescence bandwidth remains within 38 – 43 nm. These variations indicate a stable solvation environment and minimal perturbation of the electronic energy levels upon dilution. This behavior reflects a homogeneous solvation environment in which intermolecular interaction is weak and does not produce spectral broadening. This agrees with previous reports that found that BODIPY dye in polar solvents sustains stable excited-state dynamics and narrow spectral FWHM due to its rigid molecular structure [21].

The Stokes shift values (11–15 nm) indicate a small energy difference between absorption and fluorescence processes, supporting efficient radiative relaxation with minimal non-radiative loss. The minor variation in Stokes shift at intermediate concentrations may be attributed to weak solvent relaxation effects and no systematic trend indicative of aggregation or excimer formation.

Combined analysis of Figure 3 and Table 2 shows that the BODIPY dye exhibits good optical stability, high fluorescence efficiency, and negligible aggregation effects within the given concentrations. This confirms that the system provides a consistent baseline for subsequent incorporation into ZnO-based hybrid structures, confirming that fluorescence enhancement can be attributed to nanoparticle-induced electromagnetic effects.

Values represent the mean of three independent measurements (n = 3). The experimental uncertainty (RSD < 2%) is smaller than the symbol size in the corresponding plots and is visually enclosed within the data points.

The optical response and fluorescence enhancement of the ZnO/BODIPY hybrid systems are illustrated in Figure 4, while the optical parameters and enhancement metrics are summarized in Table 3.

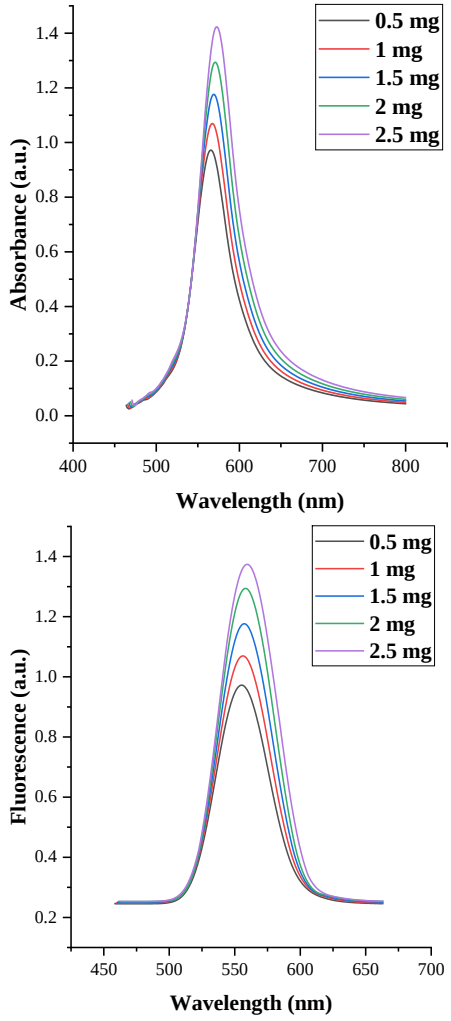


Figure 4. Ultraviolet–visible (UV–Vis) absorption and fluorescence spectra of ZnO/boron dipyrromethene (BODIPY) hybrid systems at different ZnO nanorod loadings (0.5–2.5 mg)

Figure 4 displays a clear increase in fluorescence enhancement with increasing ZnO nanorod weight. The linear behavior indicates that the optical response of the hybrid

system is dependent on ZnO loading within the range (0.5–2.5 mg). This enhancement confirms that ZnO nanorods actively contribute to amplifying the fluorescence emission of the BODIPY dye rather than acting as inactive substrates.

The optical parameters and fluorescence enhancement metrics of the prepared ZnO/BODIPY hybrid systems under different ZnO nanorod mass loadings (0.5 to 2.5 mg) are detailed in Table 3.

Table 3. Optical parameters and fluorescence enhancement factors of ZnO/boron dipyrromethene (BODIPY) hybrid systems at different ZnO nanorod loadings

ZnO Nanorod Loadings	Abs. Max. λ	FWHM Abs. (nm)	Flu. Max. λ	FWHM Flu. (nm)	Stokes Shift (nm)	Measured Enhancement Factor (EF = F/F0)	Relative Intensity (I/I0)	Localized Excitation Enhancement Factor (G/G0 = A/A0)	Radiative Decay Ratio (G/G0)/EF
0.5 mg	0.97	54	0.97	45.5	10	1.01	1.39 %	1.1	1.085
1 mg	1.07	56	1.07	46	11	1.12	11.53%	1.21	1.085
1.5 mg	1.18	58	1.18	46.5	12	1.23	22.68%	1.33	1.085
2 mg	1.29	60	1.29	47	13	1.35	34.96%	1.46	1.085
2.5 mg	1.42	62	1.42	47.5	14	1.54	53.78%	1.61	1.047

Note: Full width at half maximum (FWHM).

The results listed in Table 3 support that the fluorescence enhancement factor increases from 1.01 at 0.5 mg to 1.54 at 2.5 mg, and the relative fluorescence intensity increases, reaching 53.78% at the maximum ZnO loading. This qualitative enhancement reflects the potential influence of ZnO nanorods on the dye's photophysical environment. Similar trends reported in the literature have been tentatively attributed to localized electromagnetic field interactions; however, in the present hybrid system, this remains a plausible mechanism that warrants further direct spectroscopic and theoretical validation [22].

The localized excitation enhancement factor shows an increase from 1.1 to 1.61, indicating that the contribution to fluorescence enhancement originates from improved excitation efficiency. This behavior suggests that ZnO nanorods enhance the local electromagnetic field intensity surrounding the BODIPY molecules by increasing the probability of photon absorption. The mechanism of this enhancement may be attributed to localized electromagnetic field effects generated near the surface of ZnO nanorods, alongside potential contributions from light scattering and interfacial interactions. The increase in the localized excitation enhancement factor suggests that improved photon-harvesting efficiency might contribute to the overall fluorescence intensity. It is hypothesized that the high aspect ratio of ZnO nanorods could facilitate local light scattering and field concentration near the surface. However, without direct field-mapping or ultrafast computational simulations, these optical dynamics should be considered as proposed phenomenological contributions rather than definitive mechanisms. Also, the constant non-radiative decay ratio (~1.085) indicates a balanced contribution between excitation enhancement and radiative emission. The decrease observed at 2.5 mg (1.047) may suggest a weak aggregation effect or increased scattering losses at higher concentrations, which could reduce the efficiency of the enhancement mechanism

The increase in FWHM for absorption (54–62 nm) and fluorescence (45.5–47.5 nm) indicates increased heterogeneity in the dielectric environment upon incorporation of ZnO nanorods. This spectral broadening may arise from interfacial interactions between ZnO states and BODIPY molecules.

The Stokes shift variation from 10 to 14 nm suggests indirect modifications in excited-state relaxation due to ZnO/ BODIPY interactions. However, the small magnitude of these shifts confirms that the photophysical integrity of the BODIPY dye remains preserved in the hybrid system. Combined analysis of Figure 4 and Table 3 demonstrates that ZnO nanorods enhance the fluorescence performance of BODIPY through localized electromagnetic field effects. The increase in enhancement parameters confirms the effectiveness of ZnO nanorods as optical amplifiers, making the ZnO/BODIPY system promising for applications in fluorescence sensing, bioimaging, and advanced photonic devices.

All measurements were conducted in triplicate (n = 3). The calculated relative standard deviations (RSD) across independent runs were consistently below 2%. Due to this high experimental precision, the resulting error bars (±SD) are smaller than the plotted symbol sizes in the corresponding figures and are therefore visually enclosed within the data points.

The relationship between ZnO nanorod loading and the optical enhancement response is illustrated in Figure 5. The Figure exhibits a clear linear increasing trend, indicating a direct proportionality between ZnO concentration and the fluorescence enhancement.

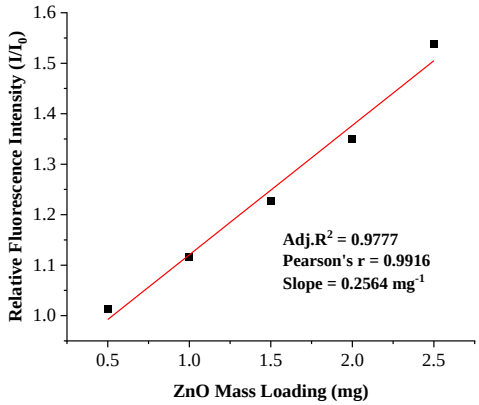


Figure 5. Linear relationship between ZnO nanorod loading and fluorescence enhancement factor in ZnO/ boron dipyrromethene (BODIPY) hybrid systems

The linearity observed in Figure 5 confirms that the fluorescence enhancement is highly controllable and dependent on the amount of ZnO nanorods incorporated into the hybrid system. This behavior suggests that the system operates within a non-saturated regime where each increase in ZnO weight contributes effectively to enhancing the optical

properties without reaching the saturation point. This linear dependence supports the control of localized electromagnetic field enhancement as the mechanism governing fluorescence amplification. As the ZnO nanorod concentration increases, the density of optically active nanostructures within the medium will increase, giving a stronger near-field effect. The absence of deviation from linearity in Figure 5 indicates that effects of nanoparticle aggregation, optical shielding, or significant scattering losses are not yet dominant within the studied concentration range (0.5–2.5 mg). This implies that the ZnO nanorods are well dispersed within the solution by ensuring efficient interaction with the dye molecules and maintaining uniform optical enhancement across the system. The deviations from linearity may occur due to aggregation effects or increased light scattering. Such effects typically lead to nonlinear optical responses in hybrid systems. Similar linear enhancement trends have been reported in published literature for ZnO-based systems, where fluorescence intensity increases with nanostructure weight due to enhanced local electromagnetic field effects and improved photon absorption efficiency [23]. The linear behavior observed in Figure 5 strongly supports the efficiency and tunability of the ZnO/BODIPY system. Combined spectroscopic observations confirm that the addition of ZnO nanorods enhances the net fluorescence intensity of BODIPY within the investigated concentrations. While localized field effects are proposed as a reasonable candidate mechanism, the observed macro-scale optical response is likely governed by a combined influence of surface interactions, light scattering, and local dielectric modification.

4. CONCLUSIONS

ZnO nanorods were synthesized using a hydrothermal method and integrated with BODIPY dye to construct highly efficient hybrid nanostructures for fluorescence enhancement applications. The structural analysis confirmed the formation of highly crystalline hexagonal ZnO nanorods with growth along the c-axis, while morphological and compositional results verified their uniform rod-like structure and high chemical purity. The optical investigations of BODIPY dye demonstrated stable photophysical properties with distinct absorption and fluorescence characteristics, narrow spectral bandwidths, and small Stokes shifts indicating high optical stability and negligible aggregation effects. These properties provided a dependable basis for assessing the hybrid system. Upon incorporation of ZnO nanorods, an enhancement in absorption and fluorescence intensities was observed. The fluorescence enhancement factor increased with ZnO loading, reaching a maximum value of 1.54 at 2.5 mg, along with an intensity enhancement of up to 53.78%. The localized excitation enhancement factor also showed a continuous increase, confirming improved light–matter interaction within the hybrid system. The observed enhancement behavior is attributed to localized electromagnetic field effects produced by ZnO nanorods, which enhance the excitation efficiency and radiative emission probability of BODIPY molecules. Additional contributions from light scattering and interfacial interactions between ZnO and dye molecules further support the enhancement mechanism. The linear dependence of fluorescence enhancement on ZnO concentration confirms the tunable nature of the hybrid system.

REFERENCES

[1] Xu, H., Akbari, M.K., Zhuiykov, S. (2021). 2D semiconductor nanomaterials and heterostructures: Controlled synthesis and functional applications. Nanoscale Research Letters, 16: 94. https://doi.org/10.1186/s11671-021-03551-w

[2] Ahmad, M.R., Ansari, A.A., Dhayal, M., Lv, R. (2025). Bandgap engineering of ZnO nanomaterials for enhanced electrochemical and photocatalytic efficiency. Renewable and Sustainable Energy Reviews, 219: 115767. https://doi.org/10.1016/j.rser.2025.115767

[3] Abed, S.M., Mohammad, S.M., Sifawa, A.A., Abdullah, M., Hassan, Z., Naser, H. (2026). Plasmon-enhanced self-powered broadband MSM photodetectors based on mixed noble metal NPs-decorated ZnO NRs on porous silicon. Solid State Sciences, 178: 108362. https://doi.org/10.1016/j.solidstatesciences.2026.108362

[4] Clarke, B., Ghandi, K. (2023). The interplay of growth mechanism and properties of ZnO nanostructures for different applications. Small, 19(44): 2302864. https://doi.org/10.1002/smll.202302864

[5] Pujara, A., Sharma, R., Bechelany, M., Mishra, Y.K., Prakash, J. (2025). Novel zinc oxide 3D tetrapod nano-microstructures: Recent progress in synthesis, modification and tailoring of optical properties for photocatalytic applications. Materials Advances, 6(7): 2123-2153. https://doi.org/10.1039/d4ma01272k

[6] Pathipati, S.R., Shah, M.N., Rao, M.N., et al. (2026). Nanoparticle-mediated growth of ZnO nanoflowers: Synthesis, growth mechanism and lead detection in electrochemical sensors. Ceramics International, 52(15): 28628-28645. https://doi.org/10.1016/j.ceramint.2026.04.393

[7] Wang, M., Zhao, W., Dong, X. (2025). Design, synthesis, and evaluation of boron dipyrromethene-based fluorescent probes targeting BRAF for melanoma diagnosis. ChemMedChem, 20(13): e202500095. https://doi.org/10.1002/cmdc.202500095

[8] Yang, Z., Liu, Y., Xie, Z., Zheng, M. (2026). Multifunctional boron-dipyrromethene platforms for disease diagnosis and therapy: Advances in bioimaging, and phototherapeutics. Journal of Photochemistry and Photobiology C: Photochemistry Reviews, 66: 100739. https://doi.org/10.1016/j.jphotochemrev.2026.100739

[9] Cordeiro, P., Menezes, V., Ebersol, C., et al. (2025). BODIPY dyes: From chalcogen-based synthesis to emerging applications and sulfur compound detection. Dyes and Pigments, 242: 112985. https://doi.org/10.1016/j.dyepig.2025.112985

[10] Gonçalves, R.C., Nogueira, M.B., Costa, S.P., Raposo, M.M.M. (2018). BODIPY derivatives: Synthesis and evaluation of their optical properties. Proceedings, 9: 10. https://doi.org/10.3390/ecsoc-22-05700

[11] Ksenofontova, K.V., Kerner, A.A., Ksenofontov, A.A., et al. (2022). Amine-reactive BODIPY dye: Spectral properties and application for protein labeling. Molecules, 27(22): 7911. https://doi.org/10.3390/molecules27227911

[12] Arrigo, A., Gangemi, C.M.A., Barattucci, A., et al. (2024). Highly efficient luminescent solar concentrators based on BODIPY derivatives. Advanced Materials Interfaces, 11(20): 2400114. https://doi.org/10.1002/admi.202400114

[13] Sharma, P., Bouffard, J., Kim, Y. (2025). A reflection on 'Aggregation-induced emission enhancement of a meso-trifluoromethyl BODIPY via J-aggregation': From fundamental discovery to versatile sensing platforms. Chemical Science, 16(45): 21147-21151. https://doi.org/10.1039/d5sc90236c
[14] Guan, Q., Fu, D.D., Li, Y.A., et al. (2019). BODIPY-decorated nanoscale covalent organic frameworks for photodynamic therapy. iScience, 14: 180-198. https://doi.org/10.1016/j.isci.2019.03.028
[15] Gao, S., Zhou, R., Samanta, S., Qu, J., Ohulchanskyy, T.Y. (2023). Recent advances in plasmon-enhanced luminescence for biosensing and bioimaging. Analytica Chimica Acta, 1254: 341086. https://doi.org/10.1016/j.aca.2023.341086
[16] Yang, L., Duan, Y., Li, Y., et al. (2026). Next-generation quantum dot fluorescent probes: Design innovations and biomedical applications. Review of Materials Research, 2: 100146. https://doi.org/10.1016/j.revmat.2026.100146
[17] Abou Zeid, S., Maquart, M., Fourdrin, C., Bastide, S., Leprince-Wang, Y. (2026). Hydrothermally grown ZnO nanowires on silicon and quartz: Multifunctional coatings with enhanced antiviral activity against SARS-CoV-2. Langmuir, 42(8): 6282-6291. https://doi.org/10.1021/acs.langmuir.5c05884
[18] Bhakar, A., Taxak, M., Rai, S.K. (2023). Significance of diffraction peak shapes in determining crystallite size distribution: A peak shape analysis procedure for pseudo-Voigt profiles and its application. Applied Crystallography, 56(5): 1466-1479. https://doi.org/10.1107/S1600576723007367
[19] Sytu, M.R.C., Hahm, J.I. (2024). Principles and applications of ZnO nanomaterials in optical biosensors and ZnO nanomaterial-enhanced biodetection. Biosensors, 14(10): 480. https://doi.org/10.3390/bios14100480
[20] Gonçalves, R.C., Belmonte-Reche, E., Pina, J., et al. (2022). Bioimaging of lysosomes with a BODIPY pH-dependent fluorescent probe. Molecules, 27(22): 8065. https://doi.org/10.3390/molecules27228065
[21] Moskaieva, O., Lebedev, M., Smortsova, Y., et al. (2023). Conformational effect on the photophysics of two BODIPY dyes in a mixture of butanol and acetonitrile: Insight from the steady-state, fluorescence time-resolved spectroscopy and TD-DFT calculations. Journal of Molecular Liquids, 382: 121877. https://doi.org/10.1016/j.molliq.2023.121877
[22] Sytu, M.R.C., Hahm, J.I. (2025). Individual ZnO–Ag hybrid nanorods for synergistic fluorescence enhancement towards highly sensitive and miniaturized biodetection. Nanomaterials, 15(8): 617. https://doi.org/10.3390/nano15080617
[23] Bartolomé, M., Villaseñor, M.J., Ríos, Á. (2025). Surface plasmon resonance optical sensors involving nanomaterials as reliable analytical tools: A critical view about performance and applications. Analytica Chimica Acta, 1382: 344693. https://doi.org/10.1016/j.aca.2025.344693